Int. J. Solids Structures Vol. 29, No. 20, pp. 2423–2440, 1992
Printed in Great Britain.

0020-7683/92 $5.00+.00

ELASTIC ANALYSIS OF THREE-DIMENSIONAL SOLIDS WITH FIBER INCLUSIONS BY BEM

P. K. BANERJEE and D. P. HENRY
Department of Civil Engineering, State University of New York at Buffalo, Amherst, NY 14260, U.S.A.

(*Received* 3 *December* 1991; *in revised form* 6 *March* 1992)

Abstract—A very efficient method of analysis for the elastic behavior of three-dimensional solids with a large number of embedded fiber inclusions has been developed. For specific applications to the analysis of cylindrical shaped fiber inclusions significant gain in efficiency can be achieved by defining these inclusions by a system of curvilinear line elements with a prescribed diameter and by assuming a variation in the traction and displacement field in the circumferential directions in terms of a trigonometric shape function together with a linear or quadratic variation along the longitudinal direction. The resulting integrals are then treated semi-analytically. A number of examples of the analysis which has been developed for composite elements are described.

INTRODUCTION

The behavior of composites under mechanical, thermal and dynamic loading is extremely complex and can only be understood if the observed behavior is interpreted in terms of micromechanical or macromechanical analyses. Such analyses must take care of the complex interaction of the individual fibers or bundles of fibers embedded in the three-dimensional matrix and must allow for increasing levels of sophistication in terms of the idealization of the fibers as well as the matrix.

It is evident that for proper analysis of composites one needs to use a numerical method that is capable of idealizing the individual fibers or individual bundles of fibers embedded within a three-dimensional matrix. The analysis must be able to take account of high stress gradients resulting from the diffusion of stress from the fiber to the matrix and must allow for the interaction between the fibers through the matrix. The boundary element method is uniquely suited for the task. BEM has proven its ability to accurately determine stress near a stress concentration. All functional quantities in a BEM system are on the boundary, therefore, allowing interaction on the interface between the matrix and the fiber to be readily described by BEM models. Further, recent developments have shown the generality and versatility of the boundary element method in analysing large two- and three-dimensional problems subjected to static, dynamic and thermal loads.

This paper details the progress made to date towards the development of a boundary element analysis designed for the elastic micromechanical and macromechanical studies of composites. The analysis is developed by expressing the surface integrals involved at the inclusion matrix interfaces in terms of trigonometric shape functions in the circumferential direction and linear or quadratic shape functions in the longitudinal direction so that the resulting integrals could be evaluated semi-analytically.

The developed analysis has been applied to a number of problems to show that it can be used for micro and macromechanical studies of composites.

ELASTOSTATIC BEM FORMULATION

The conventional boundary integral equations for elastostatic analyses are used to derive a boundary element formulation for the analysis of composite structures. The boundary integral equation written for a point in the interior of the composite matrix is modified by adding to it the boundary integral equations of each inclusion written at the same point in the composite matrix. This eventually eliminates the displacement variables

at the inclusion-matrix interface to the system, and therefore, reduces the total number of equations required for a solution of the system.

The direct boundary integral equation for the displacement at a point ξ inside an elastic body with holes is (Dargush and Banerjee, 1989; Henry and Banerjee, 1991):

$$C_{ij}(\xi)u_i(\xi) = \int_S [G_{ij}^{O}(x,\xi)t_i^{O}(x) - F_{ij}^{O}(x,\xi)u_i^{O}(x)]\,dS(x) + \sum_{n=1}^{N}\int_{S^n} [G_{ij}^{H}(x,\xi)t_i^{H}(x) - F_{ij}^{H}(x,\xi)u_i^{H}(x)]\,dS^n(x), \quad i,j = 1,2,3, \quad (1)$$

where

G_{ij}, F_{ij}	are the fundamental Kelvin tensors of the governing differential equations of the matrix of infinite extent (Banerjee and Butterfield, 1981);
C_{ij}	are constants determined by the geometry at ξ;
u_i, t_i	are displacements and tractions;
S, S^n	are the surfaces of the outer boundary of the matrix and the nth hole (left for fiber), respectively;
N	is the number of individual fibers.

Superscripts O and H identify the quantities on the outer surface of the matrix and the quantities on the surface of the hole, respectively.

The conventional boundary integral equation for displacement can also be written for each of the N fibers. For the displacement at a point ξ inside the nth fiber inclusion we can write

$$C_{ij}^{I}(\xi)u_i(\xi) = \int_{S^n} [G_{ij}^{I}(x,\xi)t_i^{I}(x) - F_{ij}^{I}(x,\xi)u_i^{I}(x)]\,dS^n(x), \quad (2)$$

G_{ij}^{I}, F_{ij}^{I}	are the fundamental Kelvin tensors of the nth fiber inclusion material of infinite extent;
C_{ij}^{I}	are constants determined by the geometry at ξ in fiber n;
u_i^{I}, t_i^{I}	are displacement and tractions associated with the nth fiber;
S^n	the surface of the nth fiber.

We next examine the interface conditions between the composite matrix and the fiber. For a perfect bond the displacement of the matrix and that of the fiber inclusion are equal and the tractions along the interface are equal and opposite:

$$u_i^{H}(x) = u_i^{I}(x), \qquad t_i^{H}(x) = -t_i^{I}(x). \quad (3a, b)$$

When the elastic modulus of the fiber is much greater than the modulus of the composite matrix, the Poisson ratio of the inclusion can be assumed to be equal to that of the matrix with little error. Although this asumption can easily be relaxed, and will be in the future, it does lead to considerable efficiency without much error in the analysis. Therefore, upon consideration of the surface normals at the interface and examination of the F_{ij} kernels, we can write the following relation for the nth inclusion

$$F_{ij}^{I}(x,\xi) = -F_{ij}^{H}(x,\xi). \quad (3c)$$

Substitution of eqns (3) into eqn (2) yields the following modified boundary integral equation for fiber inclusion "n".

$$C^{I}_{ij}(\xi)u_i(\xi) = \int_{S^n} [-G^{I}_{ij}(x,\xi)t^{H}_i(x) + F^{H}_{ij}(x,\xi)u^{H}_i(x)]\,dS^n(x). \quad (4)$$

Finally adding the N fiber inclusion eqns (4) to eqn (1) and cancelling terms, yields the modified boundary integral equation for the composite matrix

$$\bar{C}_{ij}(\xi)u_i(\xi) = \int_S [G^{O}_{ij}(x,\xi)t^{O}_i(x) - F^{O}_{ij}(x,\xi)u^{O}_i(x)]\,dS(x) + \sum_{n=1}^{N}\int_{S^n} \bar{G}^{n}_{ij}(x,\xi)t^{H}_i(x)\,dS^n(x), \quad (5)$$

where

$$\bar{G}^{n}_{ij}(x,\xi) = G^{H}_{ij}(x,\xi) - (G^{I}_{ij}(x,\xi))^n,$$

$\bar{C}_{ij}(\xi)$ are constants dependent on the geometry for a point ξ on the outer boundary and $\bar{C}_{ij}(\xi) = \delta_{ij}$ for a point ξ in the interior of the matrix.

ANALYTIC INTEGRATION AROUND A FIBER INCLUSION

The boundary element discretization of eqns (4) and (5) in the conventional manner (Banerjee and Butterfield, 1981) required a very fine discretization about the inclusion. Alternatively, a new formulation is introduced in this paper for the efficient modeling and analysis of fiber inclusions using what the authors refer to as "Inclusion Elements". These elements are defined by describing the centerline of the (curvilinear, tubular) inclusion with nodal points; defining the connectivity of the nodal points; and specifying the radius of the inclusion at each of these nodal points. The displacements and tractions at the surface of these inclusions are described using a trigonometric circular shape function in the circumferential direction and a curvilinear shape function of any order in the longitudinal direction (the present work employs both linear and quadratic shape functions for this purpose). A long inclusion (which is allowed to vary in diameter) can thus be described by a number of the "inclusion elements" connected end to end, and any such element not connected to another is assumed to be closed at the end by a circular disc.

Using the concept of the "inclusion element", the essential part of the formulation is the conversion of the two-dimensional surface integration of the inclusion (and of the hole) to a one-dimensional integration (Barone and Caulk, 1985; Dargush and Banerjee, 1989; Henry and Banerjee, 1991). In eqn (5) the integral under the summation is the integral associated with the hole and inclusion which is to be modified. To facilitate an analytic integration in the circumferential direction, the three-dimensional kernel functions are first expressed in local coordinates with the center of the coordinate system coinciding with the center of the hole and inclusion and the z axis aligned with the centerline of the inclusion. The relative translation ξ'_i is added to the field coordinate ξ_i and the rotation is applied using the appropriate vector transformation.

$$\xi_i = a_{ij}\bar{\xi}_j + \xi'_i,$$

where a_{ij} are the direction cosines between the axis of the local and global coordinate systems and the bar indicates a local variable.

The integration point x_i for a ring can now be expressed in cylindrical coordinates relative to the center of the hole and inclusion as $x_1 = R\cos\theta$, $x_2 = R\sin\theta$, $x_3 = 0$, where R represents the radius of the local inclusion, i.e. $R = (x_1^2 + x_2^2)^{1/2}$.

The normal vectors are transformed by $n_1 = n_r\cos\theta$, $n_2 = n_r\sin\theta$, $n_3 = n_z$ where n_r and n_z represent the normals of the side of the hole in local coordinates and are dependent on the change in the radius of the hole and inclusion. On the side of a straight hole $n_r = 1$ and $n_z = 0$, and on the flat surface closing the end of the hole and inclusion $n_r = 0$ and $n_z = 1$.

Next a circular shape function is employed to approximate the variation in the traction about the circumference of the hole and inclusion. The circular shape function is multiplied

and integrated with the three-dimensional $\bar{G}_{ij}^{n}$ kernal, allowing the nodal values of traction to be brought outside the integral. The shape function is expressed as (Henry and Banerjee, 1991):

$$t_i = M^{\gamma} t_i^{\gamma} \quad \text{(summation over } \gamma \text{ in implied, } \gamma = 1,2,3),$$

where

$$M^1(\theta) = \tfrac{1}{3} + \tfrac{2}{3}\cos\theta, \quad M^2(\theta) = \tfrac{1}{3} + \frac{\sqrt{3}}{3}\sin\theta - \tfrac{1}{3}\cos\theta, \quad M^3(\theta) = \tfrac{1}{3} - \frac{\sqrt{3}}{3}\sin\theta - \tfrac{1}{3}\cos\theta,$$

and t_i^{γ} is the nodal traction.

A modified circular shape function is used in the integration over the end of the hole or inclusion to ensure continuity of traction at the center of the end surface. The modified shape function is expressed as:

$$\tilde{M}^{\gamma} = aM^{\gamma} + b/3, \quad \gamma = 1,2,3, \quad a = r/R, \quad b = (R-r)/R,$$

where

R is the radius of the hole and inclusion at the end,
r is the location of the integration point as it sweeps from $r = 0$ to $r = R$.

The traction must also be transformed between the local and the global systems by $t_i = a_{ik}\bar{t}_k$ or $\bar{t}_j = a_{mj} t_m$.

The last term in eqn (5) can now be analytically integrated in the circumferential direction. For the mth hole the two integrals involved can be expressed as

$$\int_{S^m} \bar{G}_{ij}^{n}(x,\xi) t_i^{H}(x)\, \mathrm{d}s^m(x) = \int_{C^m} a_{jk} \int_0^{2\pi} \bar{G}_{ik}^{\text{local}}(R,\theta,z,\bar{\xi}) M^{\gamma} R\, \mathrm{d}\theta\, a_{il} t_l^{\gamma}\, \mathrm{d}C^m$$

$$= \int_{C^m} \bar{G}_{ij}^{\gamma}(R,z,\bar{\xi}) t_j^{\gamma}\, \mathrm{d}C^m(z),$$

where the indicated integration over C^m is now a one-dimensional curvilinear integration along the hole and $\bar{G}_{ij}^{\gamma}$ represent the semi-analytically integrated kernel functions. Note, since the transformation vector a_{ik} is independent of angle θ, it may be taken outside the $\mathrm{d}\theta$ integration. Similar semi-analytic integration is also performed in eqn (4).

The final kernel functions of the hole and inclusion obtained from the analytical integration are very lengthy and therefore are not presented in this paper. They contain functions of a large family of elliptic integrals which in general are expressed numerically by common series approximations (Abramowitz and Stegan, 1974; Byrd and Friedman, 1954; Wang, 1989; Wang and Banerjee, 1989; Henry and Banerjee, 1991).

The interior strain equation is derived from the displacement eqn (1) (or 2) by differentiation and application of the strain–displacement equations. The stresses are then found using Hooke's law. Note, the authors perform the required differentiation before the analytic circumferential integration.

Finally, an inclusion which has curvature along its length will differ in surface area about the circumference on the curved portion of the inclusion. This is neglected in the formulation since the analytical integration is performed on an axisymmetric ring in which the surface area is constant about the circumference. This error, however, is small and disappears completely on a straight tubular inclusion which is most commonly encountered.

NUMERICAL IMPLEMENTATION

The integral representations described above are accurate statements of the composite problem, however, approximations such as finite discretization and numerical integration

are necessary in order to obtain a solution to non-trivial problems. The goal of the numerical implementation of the present formulation is to obtain the most accurate and efficient implementation possible.

After the analytical integration in the circumferential direction is complete, an inclusion in a three-dimensional solid can be modeled as a two-dimensional curvilinear line element with a prescribed radius at each longitudinal node. In the discretized form the displacement boundary integral equation for an elastic body containing inclusion (eqn 4) can be expressed for a single inclusion as

$$C_{ij}^{I}(\xi)u_i(\xi) = -\sum_{p=1}^{P}\left[\int_{C^p} G_{ij}^{I\gamma}(x,\xi)N^{\alpha}(\eta)\,dC^p\right]t_i^{\alpha\gamma} + \sum_{p=1}^{P}\left[\int_{C^p} F_{ij}^{I\gamma}(x,\xi)N^{\alpha}(\eta)\,dC^p\right]u_i^{\alpha\gamma}, \quad (6)$$

where

P is the number of line elements;
$N^{\gamma}(\eta)$ represents a shape function over the curvilinear line element. Summation over γ, α, is implied;
$t_i^{\alpha\gamma}$ and $u_i^{\alpha\gamma}$ are nodal values of traction and displacement on the surface of the hole, respectively.

In a similar manner, eqn (5) can be discretized using one-dimensional shape functions over the surface of inclusion and two-dimensional shape functions over the outer surface of the body:

$$\bar{C}_{ij}(\xi)u_i(\xi) = \sum_{q=1}^{Q}\left[\int_{S^q} G_{ij}^{O}(x,\xi)L^{\beta}(\eta_1,\eta_2)\,dS^q\right]t_i^{\beta} - \sum_{q=1}^{Q}\left[\int_{S^q} F_{ij}^{O}(x,\xi)L^{\beta}(\eta_1,\eta_2)\,dS^q\right]u_i^{\beta} + \sum_{p=1}^{P}\left[\int_{C^p} \bar{G}_{ij}^{I\gamma}(x,\xi)N^{\alpha}(\eta)\,dC^p\right]t_i^{\alpha\gamma}, \quad (7)$$

where

Q is the number of surface elements on the outer surface of the composite matrix in the region;
$L^{\beta}(\eta_1,\eta_2)$ represents a two-dimensional shape function.

Summation over γ and β is implied.

It is important to note that the displacement and traction on an inclusion varies in the longitudinal as well as the circumferential direction, i.e. for displacement it varies, $u_j = M^{\alpha}N^{\gamma}u_j^{\alpha\gamma}$.

The circular shape function M^{α} has been analytically integrated into the kernel functions of eqns (6) and (7). The ends of the inclusion are assumed to be a flat surface and a one-dimensional numerical integration is carried out in the radial direction. The coefficients obtained from the integration over the ends are lumped with their respective coefficients from the integration of the side of the inclusion.

The complexity of the integral in the discretized equation necessitates the use of numerical integration for their evaluation. The steps in the integration process for a given element is outlined below:

(1) Using appropriate Jacobian transformations, a curvilinear line element or surface element is mapped on a unit line or on a flat unit cell, respectively.
(2) Depending on the proximity between the field point (ξ) and the element under consideration, there is an automatic element subdivision and additional mapping for improved accuracy.
(3) Gaussian quadrature formulae are employed for the evaluation of the discretized integral over each element (or sub-element). These formulae approximate the integral as a sum of weighted function values at designated points. The error in the approximation is dependent on the order of the (Gauss) points employed in

the formula. To minimize error while at the same time maintaining computational efficiency, optimization schemes are used to choose the best number of points for a particular combination of field point and element or subelement (Watson, 1979; Banerjee and Butterfield, 1981; Banerjee *et al.*, 1988).

(4) When the field point coincides with a node of the element being integrated, the integration becomes singular. In this case, the value of the coefficients of the F_{ij} kernel corresponding to the singular node cannot be calculated accurately by numerical integration. Instead, after the integration of all elements is complete, this value is determined so as to satisfy a rigid body displacement of the body (Banerjee and Butterfield, 1981).

After the derivation of the modified boundary integral equations and the analytical circumferential integration of the kernel functions, the next critical step in the formulation is the assembly of the inclusion in the system equations. Here, efficiency is of utmost importance. The strategy is to retain in the system only traction variables on the matrix-fiber interface. This is in contrast to a general multi-region problem where both displacement and tractions are retained on an interface. The elimination of the displacement on the interface is achieved through a backsubstitution of the inclusion equations in the system equations which are made up exclusively from equations written for the composite matrix (on the outer surface and on the surface of the holes). The procedure is described below.

Equation (7) is used to generate a system of equations for nodes on the outer surface of the composite matrix and for nodes on the surface of the holes containing the inclusions. Written in matrix form we have:

$$\text{on the matrix outer surface:} \quad \mathbf{G}^{O}\mathbf{t}^{O} - \mathbf{F}^{O}\mathbf{u}^{O} + \bar{\mathbf{G}}\mathbf{t}^{H} = 0, \tag{8a}$$

$$\text{on the matrix hole surface:} \quad \mathbf{G}^{O}\mathbf{t}^{O} - \mathbf{G}^{O}\mathbf{u}^{O} + \bar{\mathbf{G}}t^{H} = \mathbf{I}\mathbf{u}^{H}, \tag{8b}$$

where

$\mathbf{t}^{O}$ and $\mathbf{u}^{O}$ are traction and displacement vectors on the outer surface of the composite matrix;
$\mathbf{t}^{H}$ and $\mathbf{u}^{H}$ are traction and displacement vectors on the surface of the inclusion;
$\mathbf{I}$ is the identity matrix;
$\mathbf{G}^{O}$ and $\mathbf{F}^{O}$ matrices contain coefficients from the integration over the outer boundary;
$\bar{\mathbf{G}}$ matrix contains coefficients integrated about the hole/inclusion.

Our goal is to eliminate $\mathbf{u}^{H}$ from the system. To this end, eqn (6) is written for every node on an inclusion, collocating slightly outside the boundary of the inclusion [at a distance of (1.25) * (inclusion radius)] where $C_{ij}^{I}(\xi) = 0$:

$$\mathbf{F}^{I2}\mathbf{u}^{I} = \mathbf{G}^{I2}\mathbf{t}^{I}.$$

Superscript I2 identifies the equations written at points located slightly outside the boundary of the inclusions.

Noting $\mathbf{u}^{H} = \mathbf{u}^{I}$ and $\mathbf{t}^{H} = -\mathbf{t}^{I}$ we have

$$\mathbf{F}^{I2}\mathbf{u}^{H} = -\mathbf{G}^{I2}\mathbf{t}^{H}. \tag{9}$$

Post-multiplying eqn (8b) by the $\mathbf{F}^{I2}$ matrix in eqn (9) yields

$$\mathbf{F}^{I2}\mathbf{G}^{O}\mathbf{t}^{O} - \mathbf{F}^{I2}\mathbf{F}^{O}\mathbf{u}^{O} + \mathbf{F}^{I2}\bar{\mathbf{G}}\mathbf{t}^{H} = \mathbf{F}^{I2}\mathbf{u}^{H}. \tag{10}$$

Equation (9) can now be set equal to eqn (10) and the final form of the system is derived:

$$\text{on outer surface:} \quad \mathbf{G}^{O}\mathbf{t}^{O} - \mathbf{F}^{O}\mathbf{u}^{O} + \bar{\mathbf{G}}\mathbf{t}^{H} = \mathbf{O},$$

$$\text{on hole:} \quad \mathbf{F}^{I2}\mathbf{G}^{O}\mathbf{t}^{O} - \mathbf{F}^{I2}\mathbf{F}^{O}\mathbf{u}^{O} + (\mathbf{F}^{I2}\bar{\mathbf{G}} + \mathbf{G}^{I2})\mathbf{t}^{H} = \mathbf{O}. \tag{11}$$

At every point on the outer surface, either the traction or the displacement is specified and on the surface of the inclusion only the tractions are retained. Therefore, the number of equations in the system are equal to the final number of unknowns. After the solution of eqn (11), eqn (8b) is used to determine the displacement at the matrix–inclusion interface. It should be noted that since the displacement about a particular inclusion is present only in the inclusion equation corresponding to that matrix–inclusion interface, backsubstitution can be performed one inclusion at a time in a more efficient manner than backsubstitution for all inclusions at once. Further, nowhere in the assembly process is a matrix inversion necessary.

When the composite matrix is divided into a multi-region model, the above inclusion assembly is performed for each region independently. Thereafter, equilibrium and compatibility conditions are invoked at common interfaces of the substructured matrix composite. After collecting together the known and unknown boundary quantities, the final system can be expressed as

$$\mathbf{A}^b\mathbf{x} = \mathbf{B}^b\mathbf{y}, \tag{12}$$

where

x is the vector of unknown variables at outer boundary and unknown tractions along the inclusion/matrix interface;
y is the vector of known variables on the outer boundary of the composite matrix;
$\mathbf{A}^b\mathbf{B}^b$ are the coefficient matrices.

Standard substructured Gaussian elimination (Banerjee *et al.*, 1988) procedures are used to solve the unknowns in eqn (12).

INTERIOR QUANTITIES

Once all of the displacements and tractions are known on the matrix outer surface and on the matrix–inclusion interface, interior quantities of displacement, stress and strain can be determined at any point in the composite matrix or inclusion. For displacement, either the conventional boundary displacement integral eqn (1) or (2) can be employed or alternatively the modified eqns (4) or (5) can be used.

The interior stresses can be evaluated from the discretized form of the interior equations:

$$\sigma_{ij}^N(\xi) = \sum_{q=1}^{Q}\left[\int_{S^q} E_{kij}^{\mathrm{O}}(x,\xi)L^\beta(\eta,\eta_2)\,\mathrm{d}S^q(x)\right]t_k^\beta - \sum_{q=1}^{Q}\left[\int_{S^q} D_{kij}^{\mathrm{O}}(x,\xi)L^\beta(\eta,\eta_2)\,\mathrm{d}S^q(x)\right]u_k^\beta$$
$$+\sum_{p=1}^{P}\left[\int_{C^p} E_{kij}^{\mathrm{H}\gamma}(x,\xi)N^\alpha(\eta)\,\mathrm{d}C^p(x)\right]t_k^{\alpha\gamma} - \sum_{p=1}^{P}\left[\int_{C^p} D_{kij}^{\mathrm{H}\gamma}(x,\xi)N^\alpha(\eta)\,\mathrm{d}C^p(x)\right]u_k^{\alpha\gamma}, \tag{13}$$

in which

$$E_{kij} = \frac{2\mu\nu}{1-2\nu}\delta_{ij}\frac{\partial G_{kl}}{\partial \xi_l} + \mu\left(\frac{\partial G_{ki}}{\partial \xi_j} + \frac{\partial G_{kj}}{\partial \xi_i}\right), \tag{14a}$$

$$D_{kij} = \frac{2\mu\nu}{1-2\nu}\delta_{ij}\frac{\partial F_{kl}^n}{\partial \xi_l} + \mu\left(\frac{\partial F_{ki}}{\partial \xi_j} + \frac{\partial F_{kj}}{\partial \xi_i}\right). \tag{14b}$$

A similar equation could be derived if stresses are required inside an inclusion. Equation (13) is, of course, developed from (1). Since strong kernal singularities appear when (13) is written for outer boundary points, an alternate procedure is therefore needed to determine surface stress. This alternate scheme exploits the interrelationships between displacement, traction, and stress and can be expressed as:

$$\sigma_{ij}n_j(\xi) = L^\beta(\eta_1,\eta_2)t_i^\beta, \qquad \sigma_{ij}(\xi) - \frac{D^e_{ijkl}}{2}(u_{k,l}(\xi)+u_{l,k}(\xi)) = 0, \tag{15a, b}$$

$$\frac{\partial x_j}{\partial \eta_\zeta}u_{i,j}(\xi) = \frac{\partial L^\beta(\eta_1,\eta_2)}{\partial \eta_\zeta}u_i^\beta, \tag{15c}$$

where

$$D^e_{ijkl} = \lambda\delta_{ij}\delta_{kl}+2\mu\delta_{ik}\delta_{jl}.$$

Equations (15) form an independent set that can be solved numerically for $\sigma_{ij}(\xi)$ and $u_{i,j}(\xi)$ completely in terms of known nodal quantities. Notice, however, that shape function derivatives appear in (15c), thus constraining the representation of stress on the surface element to something less than the variation used for displacement.

EXAMPLES OF FIBER COMPOSITE ANALYSIS

A number of examples are presented to verify and demonstrate the applications of the composite formulation. In the discretization diagrams of models containing the inclusion, a double line is used to indicate the centerline of the inclusion elements. The lengths of these elements are shown in proper proportion for the three-dimensional views, however, the radii of the inclusions are not indicated on these diagrams. The double line is a symbolic representation of the fiber inclusion elements and does not in any way indicate the diameter. Refer to the example description for the values of the radii.

Throughout this section consistent units are used in the definition of the examples. This means all lengths are defined in the same units and the tractions and the elastic moduli are defined in terms of these lengths as force/length^2. No confusion should arise since the results are reported as non-dimensional quantities.

Cube with a single inclusion

The first test of the formulation is on a unit cube with a single inclusion of radius 0.1 through the center of the cube. The cube is subjected to tension in the direction perpendicular to the inclusion. It has a modulus of 100.0 and a Poisson ratio of 0.3. Consistent units are used for all information described in this problem. An inclusion with two different moduli of 1,000 and 10,000 is studied. The Poisson ratio of the inclusion is assumed to be the same as that of the cube.

The problem is analysed by both the present formulation and by a full three-dimensional multi-region BEM approach. As shown in Fig. 1, the model for the fiber inclusion

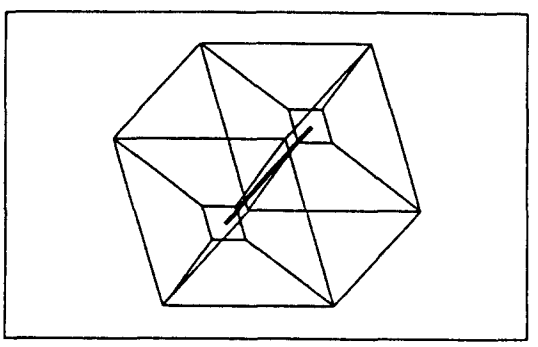

Fig. 1. Discretization of an inclusion in a unit cube utilizing quadratic inclusion elements.

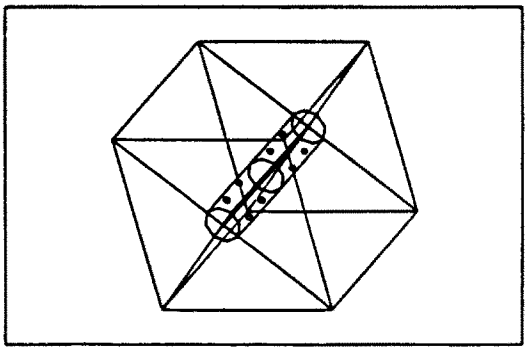

Fig. 2. Full three-dimensional, multi-region discretization of an inclusion in a unit cube.

formulation consists of 14 quadratic boundary elements and the fiber contains three quadratic inclusion elements. The two-region, three-dimensional model shown in Fig. 2 contains 20 quadratic boundary elements in the first region and 16 in the second. Note nine-noded elements are used in describing the inclusion and hole to accurately capture the curvilinear geometry.

In Fig. 3, the profile of the end displacement of the cube under a uniform normal traction of 100.0 (in parallel with the inclusion) is shown. The present formulation is in good agreement with the full three-dimensional results for $E_i/E = 10$. For the case $E_i/E = 100$, the inclusion formulation exhibits less stiffness than the 3-D results. This difference is attributed to the way the load is distributed from the inclusion to the composite matrix. In the full 3-D model, the applied traction and the resulting reactions at the fixed end act directly on the end of the inclusion. In the composite formulation, the inclusion is assumed not to intersect the boundary surface and therefore the inclusion is moved back slightly from the end of the cube. A small error therefore gets introduced in the composite formulation due to the end effects of the inclusion.

In Fig. 4, the stress distribution through the center of the cube (from A to B as indicated in the figure) is shown. Again the results are very good for $E_i/E = 10$, and deviates slightly from the full 3-D results in the second case.

Lateral behavior of a cube with multiple inclusions

Existing methods of analysis of composite material based on mechanics of materials have been relatively successful in predicting the behavior of composite material for loading in the longitudinal direction. The properties perpendicular to the direction of the fibers are

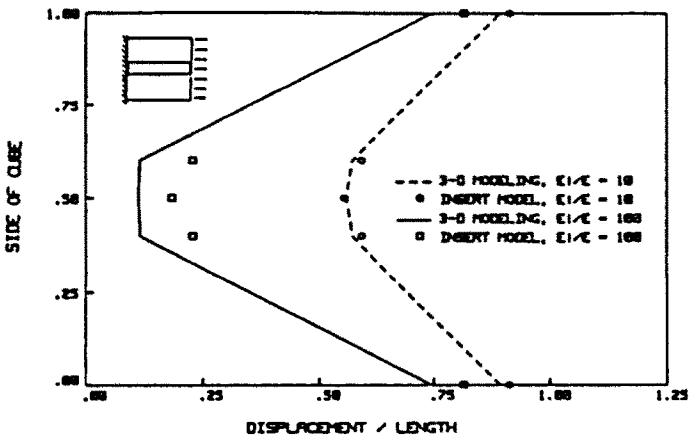

Fig. 3. Comparison of displacement profiles between the full 3-D model and the inclusion model for the end of a cube in tension.

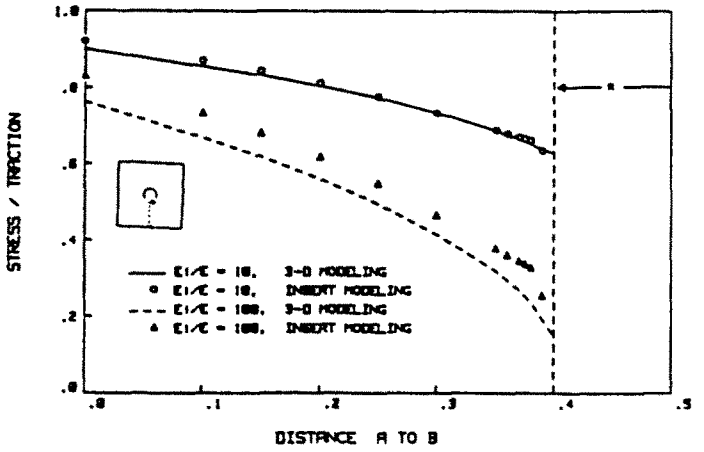

Fig. 4. Axial stress through the cross-section of a unit cube in tension with a single inclusion in parallel with the loading.

not so readily predictable by present means. The focus of the present example concerns this lateral behavior.

Four cubes (Fig. 5) with one, two, five and nine inclusions are fixed with a roller boundary condition on one side and subjected to a uniform traction, perpendicular to the inclusion axis. The material properties for the inclusion and the matrix respectively, given in consistent units, are

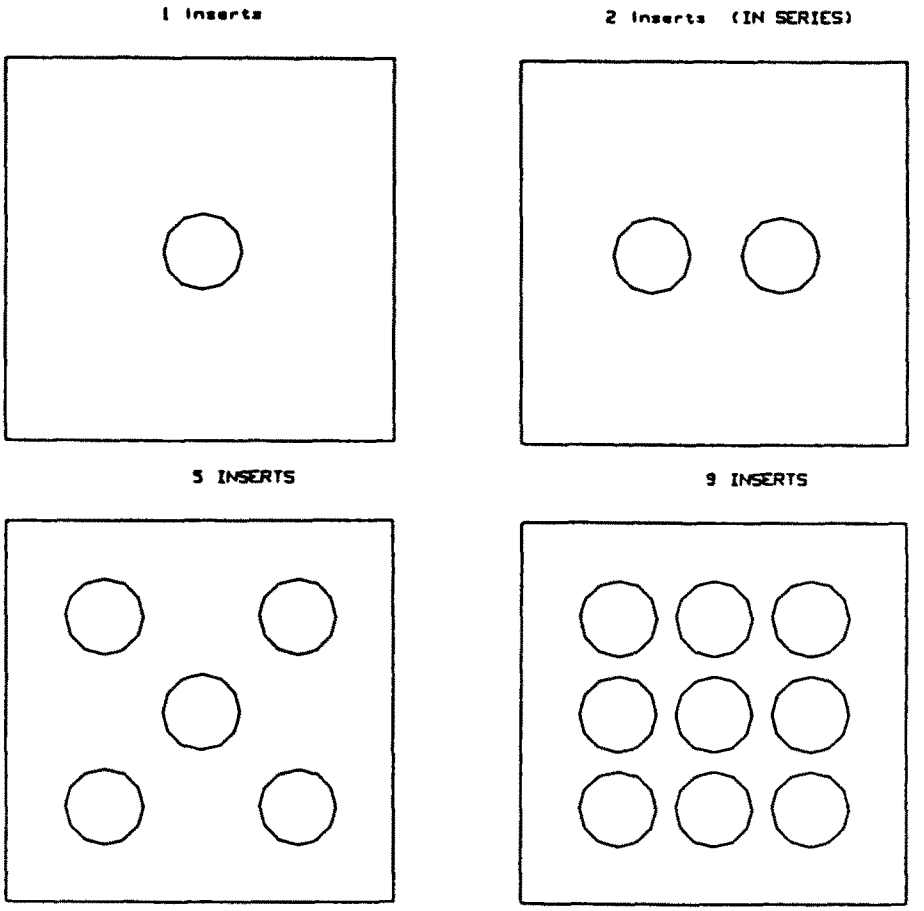

Fig. 5. Arrangement of multiple inclusions in a unit cube subjected to lateral tension.

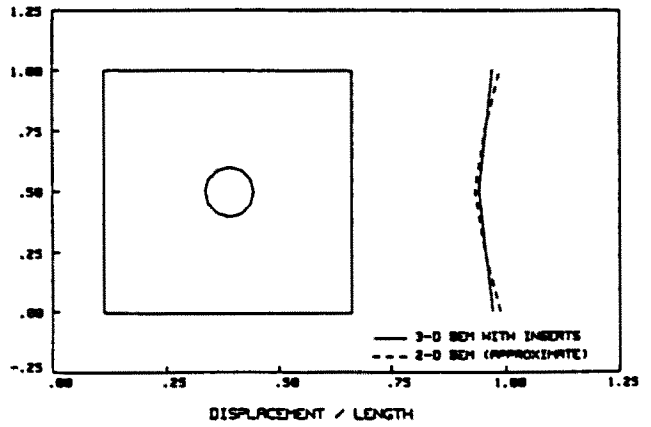

Fig. 6. Displacement profile of a cube with a single inclusion under lateral tension.

$$E^i = 1000, \quad E^m = 100, \quad \nu^i = 0.3, \quad \nu^m = 0.3.$$

For the cube with one and two inclusions, the boundary mesh consists of two quadratic surface elements on each lateral side and four elements on the top and bottom. For the cubes with five and nine inclusions, one additional element was added to the side with the applied traction and to the side with the roller boundary condition. The top and bottom faces contain six elements to match the pattern of the sides. In all cases, each inclusion was modeled using three one-dimensional quadratic elements.

The profile for the end displacement of the cube with one inclusion and five inclusions are shown in Figs 6 and 7. The results are seen to be in good agreement with the two-dimensional results. The 2-D results are approximations since plane stress is assumed. The 3-D solutions for the one inclusion are within 2% of the 2-D solution and within 3% for the case of five inclusions.

Figure 8 shows the average end displacements for the one, two, five and nine inclusions. Results once again show good agreement with 2-D results. For one, two and five inclusions, the solutions are within 2% of the 2-D results and 6% for the case of nine inclusions where the volume ratio is 28.2%. The result is also displayed in a plot of Effective Modulus vs inclusion Volume Ratio in Fig. 9. The effective modulus is defined as the average stress/average strain. The three-dimensional results follow closely to the two-dimensional solution.

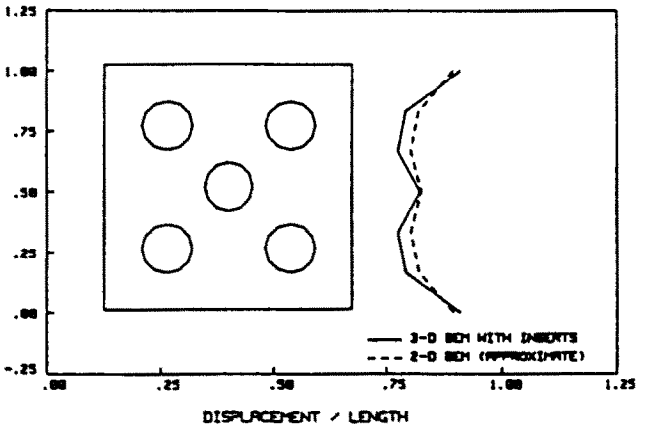

Fig. 7. Displacement profile of a cube with five inclusions under lateral tension.

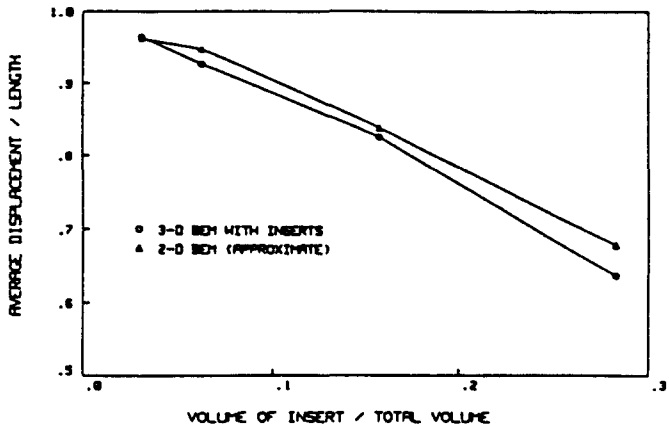

Fig. 8. Average end displacement of a cube under tension vs the volume of inclusion to total volume ratio.

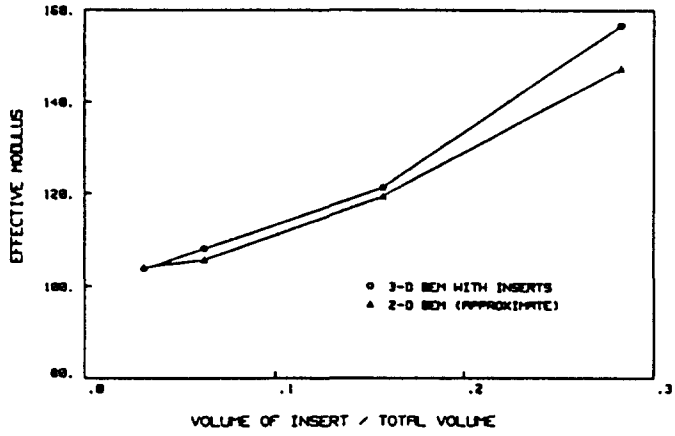

Fig. 9. Effective transverse modulus of a cube as a function of inclusion volume to total volume.

Thick cylinder with circumferential inclusions

The strength of a cylinder under internal pressure can be increased by adding stiff circumferential inclusions. In the present example, a three-dimensional, open ended thick cylinder is considered. The inner and outer radii of the cylinder are 10 and 20 respectively, the thickness is 2 and the radius of the fully-bonded inclusion is 0.5. By using roller boundary conditions on the faces of symmetry, only a 15° slice of the thick cylinder is modeled. As shown in Fig. 10, 16 eight-noded quadratic boundary elements are used to define the sides

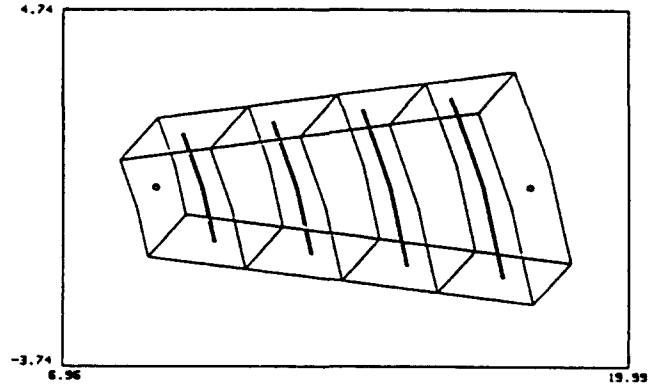

Fig. 10. Discretization of a thick cylinder with four inclusions utilizing inclusion elements.

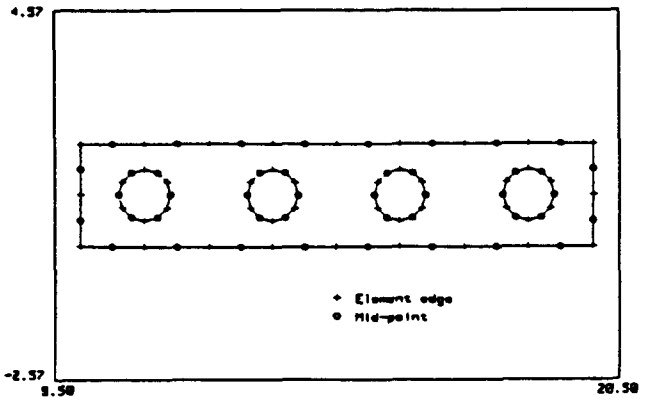

Fig. 11. Axisymmetric multi-region, discretization of a thick cylinder with four inclusions.

of the model, a nine-noded element is used on both the internal and external faces of the cylinder, and three inclusion elements are used per inclusion. Note, the inclusions in this problem are curvilinear in geometry. The elastic modulus of the cylinder is assumed to be 100, and the effect of inclusions with five different moduli of 100, 250, 500, 750 and 1000 is studied. The Poisson ratio is 0.3 for both the composite matrix and inclusion, and the internal pressure in the cylinder is 100.

Results from a multi-region, axisymmetric BEM analysis (Henry *et al.*, 1987) were used for comparison with the 3-D inclusion results of the present example. The axisymmetric model consists of 20 quadratic boundary elements on the outer surface, and six boundary element per hole and inclusion (Fig. 11). The radial displacement through the thick cylinder along the top face is shown in Fig. 12 for all five moduli. The displacement for the composite with low E_i/E ratios are in good ageement with the axisymmetric results, and diverge slightly for higher E_i/E ratios. In Fig. 13, the circumferential stress is shown for the same points along the top edge. This stress is smooth for the homogeneous case ($E_i/E = 1.0$) and exhibits increasing fluctuations as the E_i/E ratio increases and the fibers take on more of the load. The circumferential stress of the 3-D inclusion model is in good ageement with the axisymmetric results for all cases. In Fig. 14, the radial stress is displayed for the two models. The fibers have little effect on this stress and the curves of the five moduli for both approaches lie in close proximity.

Cube with multiple inclusions with random orientation

In an attempt to analyse a material with a random fiber structure, cubes with multiple fibers oriented in random directions are studied. The cubes are of unit length and have four

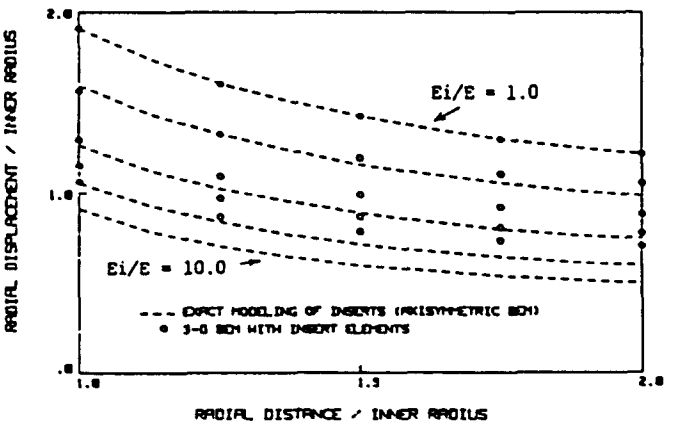

Fig. 12. Radial displacement through a pressurized thick cylinder with circumferential inclusions for $E_i/E = 1.0, 2.5, 5.0, 7.5, 10.0$.

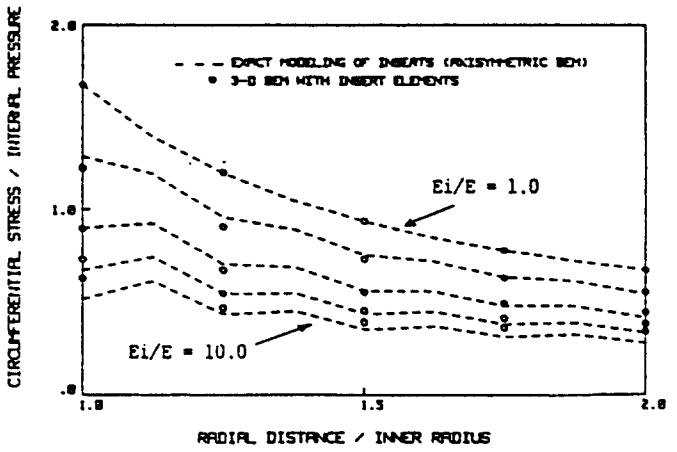

Fig. 13. Circumferential stress through a pressurized thick cylinder with circumferential inclusions for $E_i/E = 1.0, 2.5, 5.0, 7.5, 10.0$.

boundary elements per side (Fig. 15a). Randomly oriented fibers of variable length with radii of 0.05 are placed in five cubes in quantities of 5, 10, 15, 20 and 25 (Figs 15b–f). Three cases of material properties are considered for each cube. The modulus of the composite matrix is 100 for all cases, however, the modulus of the fibers are 500, 10,000 and 200,000 for the three cases studied. Poisson's ratio is uniformly 0.3 throughout. Roller boundary conditions are employed on three adjacent sides and a uniform normal traction of 100 is applied to a fourth face.

The normal end displacement at the center of the face on the side with the applied traction is plotted against the number of inclusions in a cube for the three materials (Fig. 16). The displacement decreases with increasing number of fibers per cube and increasing E_i/E values as expected.

A beam with reinforcement in bending

In the last example, the applicability of the present formulation to the study of the micromechanical and macromechanical behavior of composites is apparent. The present formulation, however, is equally applicable to typical problems encountered by civil engineers. Reinforced concrete can now be modeled exactly as a three-dimensional body and studied in detail for the first time. The present example considers a reinforced concrete beam. Here the concrete plays the role of the composite matrix and the reinforcement bars play the role of the fiber. In Fig. 17, a $4 \times 1 \times 1$ beam with four fibers is modeled using 28 quadratic boundary elements. The effect of the ratio of fiber modulus to matrix modulus

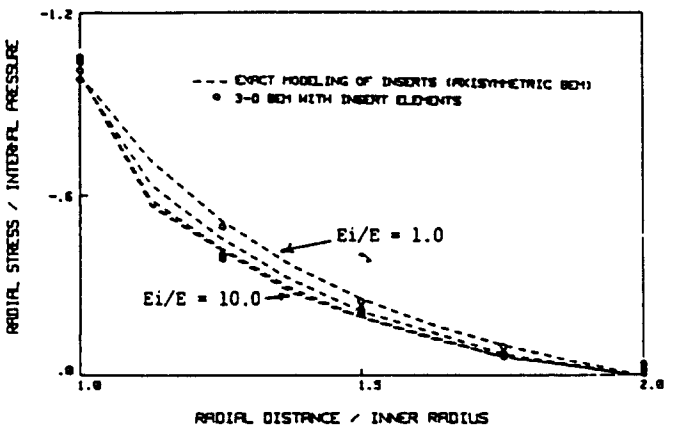

Fig. 14. Radial stress through a pressurized thick cylinder with circumferential inclusions for $E_i/E = 1.0, 2.5, 5.0, 7.5, 10.0$.

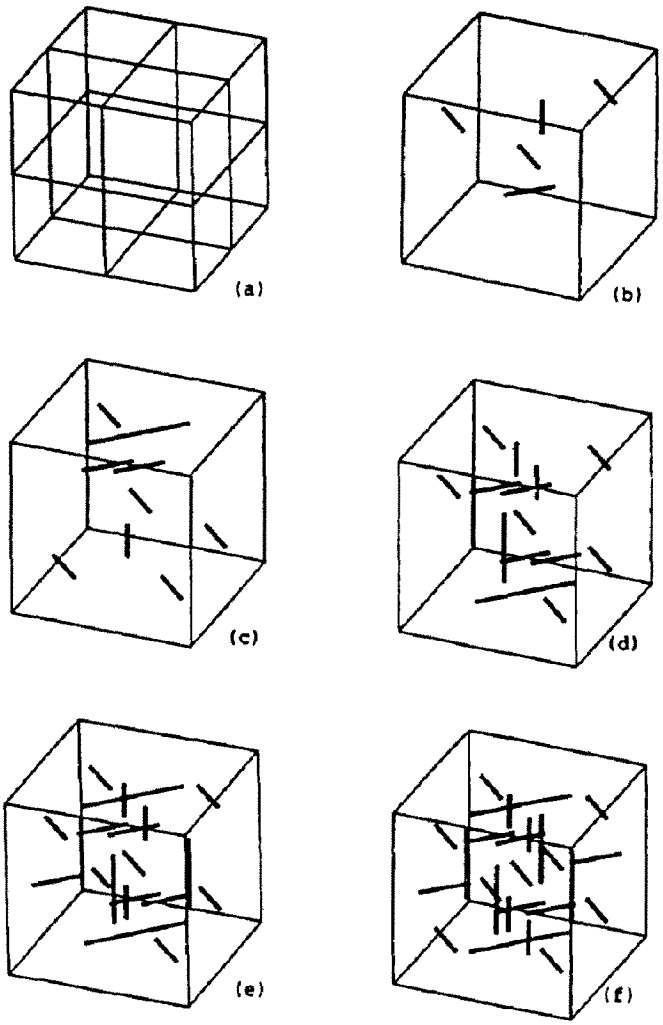

Fig. 15. (a) Surface discretization of a unit cube used in the study of random oriented inclusions. (b-f) Orientation of variable length inclusions within unit cubes containing 5, 10, 15, 20 and 25 inclusions, respectively.

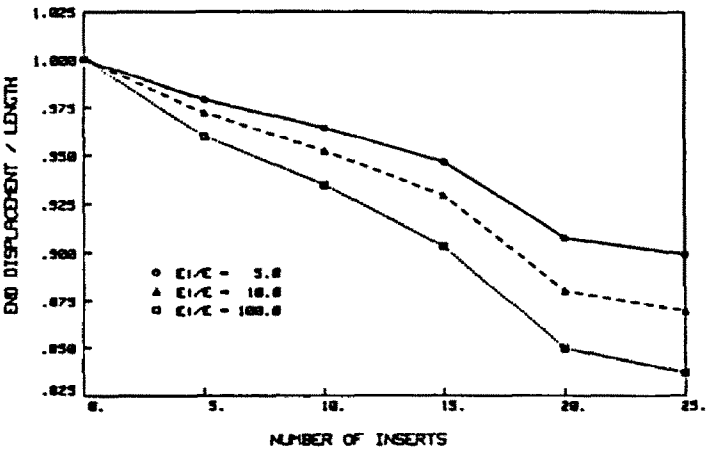

Fig. 16. End displacement of a unit cube with random oriented inclusions of $E_i/E = 5.0$, 10.0 and 100.0.

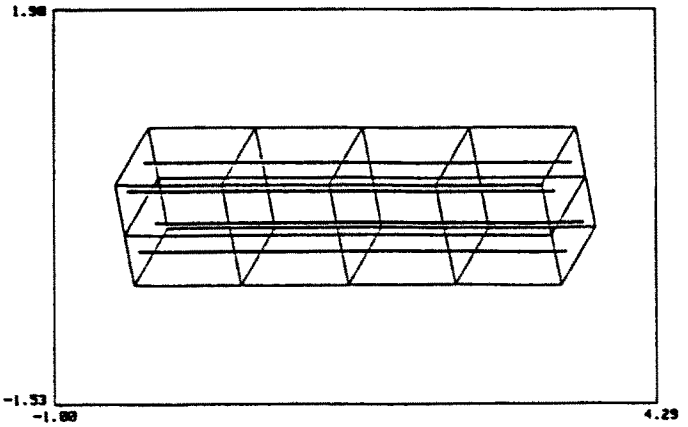

Fig. 17. Discretization of a reinforced beam utilizing quadratic inclusion elements to model the four inclusions.

(E_i/E) is studied for a range of values between 1 and 100. The Poisson ratio is 0.3 for both the beam and reinforcement.

The beam is completely fixed at one end and a downward shear traction of 100 is applied to the other end. The non-dimensional vertical displacement of the end obtained from the present analysis is shown in Fig. 18 as a function of E_i/E. The non-dimensional displacement is defined as the end displacement of the reinforced beam divided by the displacement of a homogeneous beam under similar boundary conditions.

The end displacement obtained from the mechanics of material solution is also displayed in Fig. 18 in a non-dimensional form. The curvature of the two plots are very similar but differ in magnitude. This difference is attributed to the fact that although the mechanics of material solution accounts for the stiffening due to the fibers, it does not include the effect of interaction between individual fibers.

Laminated fiber composite

A laminated composite fabricated from a fiber composite material is shown in Fig. 19. The fiber composite is constructed with a single row of fully-bonded fibers oriented in the same direction. A two-ply laminate is then constructed from the fiber composite with the fibers of the two layers oriented at 90° angles. A boundary element model created for the study of this material is shown in Fig. 20. A small slice containing two fibers in each layer

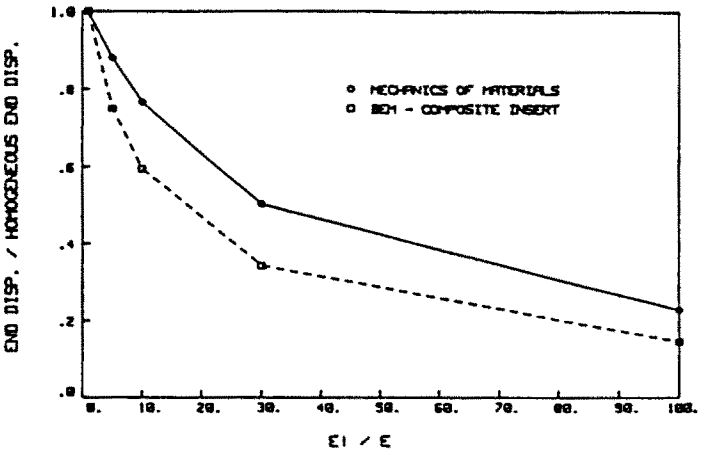

Fig. 18. Non-dimensionalized vertical end displacement of a reinforced beam in bending vs the modulus of the inclusion over modulus of the beam.

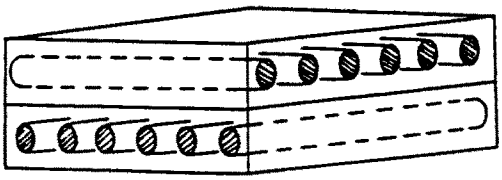

Fig. 19. Laminate–fiber composite.

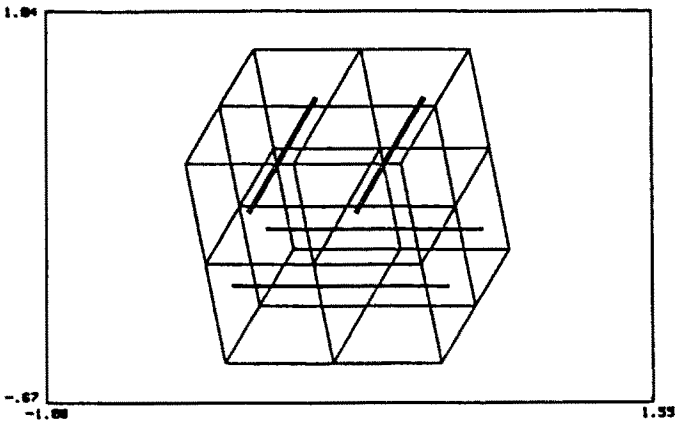

Fig. 20. BEM discretization of a laminate–fiber composite.

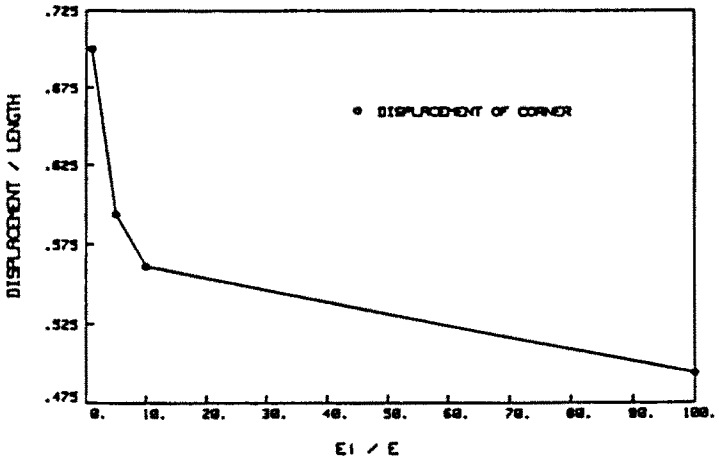

Fig. 21. Lateral displacement of a point at the corner of the interface of a laminate–fiber composite under bi-axial tension.

is used. The model consists of two regions. The outer surface of each region is modeled with 16 quadratic boundary elements and each fiber contains two quadratic inclusion elements. The interface between the two regions is assumed to be a perfect bond, however, the present analysis can easily be extended for sliding and spring connections.

The composite structure is subjected to biaxial tension. This is accomplished with normal tractions of 100 applied to two adjacent roller boundary conditions applied to the opposite ends. The elastic modulus of the composite matrix of both regions are assumed to be 100, and the moduli of the inclusion vary between 100 and 10,000. The Poisson ratio is 0.3 for both the composite matrix and fibers at all times.

Figure 21 displays one component of inplane displacements as a function of modulus ratio for a point on the interface at the corner of the plate adjacent to the sides with the

applied traction. The material exhibits less displacement as the modulus is increased, as expected.

CONCLUSIONS

An approximate BEM formulation for the efficient 3-D elastic analysis of solids with inclusions is presented. The analysis is efficient as well as reasonably accurate for a range of problems when compared with conventional multiregion modeling. One of the major advantages of this formulation lies in the fact that the locations and arrangements of these inclusions can be altered without rebuilding the BEM discretization of the outer boundary. It is also possible to store the major part of the boundary element coefficients and supplement them with new integrated coefficients for the altered design for reassembly and solution at a fraction of the original cost. The present implementation includes all of these advanced features.

Acknowledgements—The authors would like to extend their thanks to Dr Gary Dargush for his helpful discussions pertaining to the present work. The present analysis has been developed for inclusion in GPBEST and BEST-CMS engineering analysis systems. Financial support for the work was provided by NASA Lewis Center under the grant number NAG3-888. The authors are indebted to Dr C. Chamis and Mr D. Hopkins of NASA Lewis Center for their support and encouragement.

REFERENCES

Abramowitz, M. and Stegun, I. A. (1974). *Handbook of Mathematical Functions*. Dover, New York.

Banerjee, P. K. and Butterfield, R. (1981). *Boundary Element Methods in Engineering Science*. McGraw-Hill, London.

Banerjee, P. K., Wilson, R. B. and Miller, N. (1988). Advanced elastic and inelastic stress analysis of gas turbine engine structures by BEM. *Int. J. Numer. Meth. Engng* **26**, 393–411.

Barone, M. R. and Caulk, D. A. (1985). Special boundary integral equations for approximate solution of potential problems in three-dimensional regions with slender cavities of circular cross-section. *IMA J. Appl. Math.* **35**, 311–325.

Byrd, P. F. and Friedman, M. D. (1954). *Handbook of Elliptic Integrals for Engineers and Physicists*. Springer, Berlin.

Dargush, G. F. and Banerjee, P. K. (1989). Advanced development of the boundary element method for steady-state heat conduction. *Int. J. Numer. Meth. Engng* **28**, 2123–2142.

Henry, D. P. and Banerjee, P. K. (1991). Elastic analysis of three-dimensional solids with small holes by BEM. *Int. J. Numer. Meth. Engng* **31**(2), 369–384.

Henry, D. P., Pape, D. and Banerjee, P. K. (1987). New axisymmetric BEM formulation for body forces using particular integrals. *J. Engng Mech.* ASCE **113**(5), 671–688.

Wang, H. C. (1989). A general purpose development of BEM for axisymmetric solids. Ph.D. Dissertation, State University of New York at Buffalo.

Wang, H. C. and Banerjee, P. K. (1989). Multi-domain general axisymmetric stress analysis by BEM. *Int. J. Numer. Meth. Engng* **28**, 2065–2083.

Watson, J. O. (1979). Advanced implementation of the BEM for two and three-dimensional elastostatics. In *Developments in BEM* (edited by P. K. Banerjee and R. Butterfield), Vol. 1, pp. 31–63. Elsevier Applied Science, London.